

## Topology Comparison of Superconducting Generators for 10-MW Direct-Drive Wind Turbines

### Cost of Energy Based

Liu, Dong; Polinder, Henk; Abrahamsen, Asger Bech; Ferreira, Bram

#### Publication date

2016

#### Published in

2016 Applied Superconductivity Conference

#### Citation (APA)

Liu, D., Polinder, H., Abrahamsen, A. B., & Ferreira, B. (2016). Topology Comparison of Superconducting Generators for 10-MW Direct-Drive Wind Turbines: Cost of Energy Based. In *2016 Applied Superconductivity Conference*

#### Important note

To cite this publication, please use the final published version (if applicable).  
Please check the document version above.

#### Copyright

Other than for strictly personal use, it is not permitted to download, forward or distribute the text or part of it, without the consent of the author(s) and/or copyright holder(s), unless the work is under an open content license such as Creative Commons.

#### Takedown policy

Please contact us and provide details if you believe this document breaches copyrights.  
We will remove access to the work immediately and investigate your claim.

# Topology Comparison of Superconducting Generators for 10-MW Direct-Drive Wind Turbines: Cost of Energy Based

Dong Liu, *Student Member, IEEE*, Henk Polinder, *Senior Member, IEEE*,  
Asger B. Abrahamsen, and Jan A. Ferreira, *Fellow, IEEE*

**Abstract**—Superconducting synchronous generators (SCSGs) are being proposed for 10-MW direct-drive wind turbines, because of their advantages of low weight and compactness. So far, however, there has not been a commonly accepted design philosophy of SCSGs and various possibilities with many trade-offs remain for study. Partially SCSGs are considered a starting point since excessive AC losses in armature windings can be avoided. Many topologies can be applied to partially SCSGs and may significantly affect the performance indicators (PIs) of a wind turbine. Since cost of energy (CoE) is usually used as a key PI to evaluate the feasibility of an SCSG in wind turbine applications, this paper compares twelve topologies using  $MgB_2$  wires regarding the capital CoE as well as other resulting PIs. These topologies cover most possibilities for a radial-flux SCSG and four scenarios are investigated regarding the used  $MgB_2$  wire. The comparison results shows clear trends of these PIs over the twelve topologies and can be used as a reference for designing an SCSG for large direct-drive wind turbines.

**Index Terms**—Direct drive,  $MgB_2$ , performance, superconducting generator, topology, wind turbine.

## I. INTRODUCTION

**S**UPERCONDUCTING synchronous generators (SCSGs) are drawing more attention for 10-20 MW direct-drive wind power conversion [1], because they can be lightweight and compact and reduce the cost of energy (CoE) of the wind turbine [2]-[4]. Due to the high magnetic field production by superconducting (SC) coils, many possibilities exist for designing an SCSG. The SC coils can be applied only in the DC field winding or also in the AC armature winding. A commonly applied approach is to use an SC field winding at a low temperature with a copper AC armature winding at an ambient temperature [5]-[8]. In such so-called partially SCSGs, excessive AC losses in the armature winding can be avoided and the feasibility of SCSGs increases. Among typical superconductor types,  $MgB_2$  could be a starting point as a low-CoE possibility. This superconductor type is usually for operating temperatures of 10-20 K. It is not as expensive as high temperature superconductors but requires less rigorous cryogenic cooling than low temperature superconductors.

For a partially SCSG design, many topologies can be considered from the perspective of electromagnetics. A topology

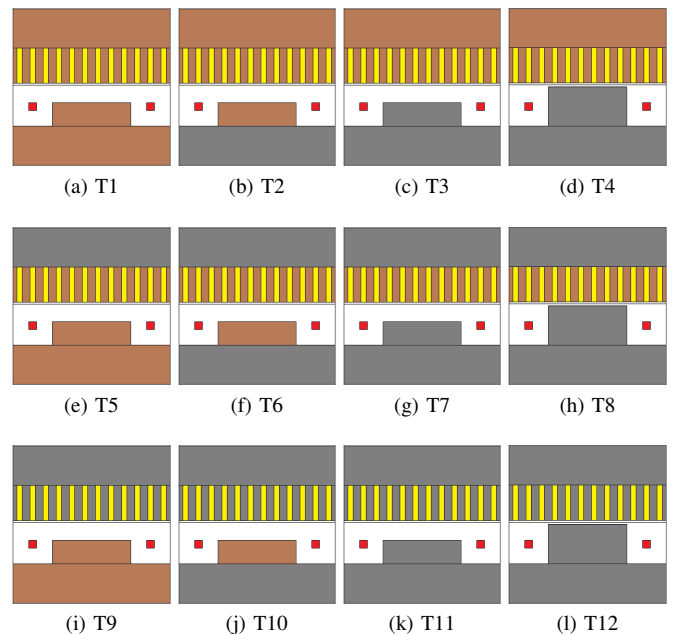


Fig. 1. Twelve topologies to be compared. Red: SC field winding. Yellow: copper armature winding. Brown: non-magnetic core. Gray: iron core.

differently combine iron and non-magnetic cores in the rotor back core, rotor pole core, stator tooth and stator yoke. They differ in the magnetic reluctance of an electrical machine. Choice of topology could significantly change the cost and efficiency of an SCSG and consequently affect the capital CoE of a wind turbine employing this SCSG.

This paper considers twelve topologies employing  $MgB_2$  in the field winding, as listed and sketched in Fig. 1, which cover most of the applicable radial-flux possibilities. Some of them have already been proposed in the literature or industry. This paper compares these topologies regarding the capital CoE of a 10-MW direct-drive wind turbine. This paper only focuses on the capital CoE as the key performance indicator (PI). The other costs, e.g. installation, operation and maintenance costs, are not taken into account since the capital CoE should be evaluated in first place to identify promising candidates which then move onto further evaluations.

Since superconductor technology is fast developing, only using the unit cost and performance of currently available  $MgB_2$  superconductors could be too limited to provide long-

D. Liu, H. Polinder, and J. A. Ferreira are with the Department of Electrical Sustainable Energy, Delft University of Technology, NL-2628 CD Delft, Netherlands. E-mail: d.liu-1@tudelft.nl.

A. B. Abrahamsen is with DTU Wind Energy, Technical University of Denmark, DK-4000 Roskilde, Denmark.

term trends of topology comparison. Thus, four scenarios for the unit cost and performance of  $MgB_2$  superconductors are taken into the comparison of PIs.

Moreover, for fair comparison, all the topologies are optimized for their minimum capital CoEs. The capital cost of each wind turbine component is estimated using the reference 10-MW turbine from the INNWIND.EU project and other capital costs are estimated based on the available literature.

## II. GENERATOR TO BE STUDIED

### A. Basic Characteristics

The partially SCSG for this study is required for a 10 MW direct-drive wind turbine defined by the INNWIND.EU project [1]. The rated speed is 9.6 rpm. The turbine rotor has a diameter of 178 m and its optimum tip speed ratio is 7.5. The maximum power coefficient of the turbine is 0.476. The air gap diameter of the SCSG is set to 6 m to obtain a compact size. The rotating part of the SCSG can be either the field winding or the armature winding since the choice will not change the results. The rated current density in the armature winding is 3 A/mm<sup>2</sup> and the armature slot filling factor is 0.6. The electrical loading limited below 75 kA/m (RMS) is to enable forced-air cooling on the armature winding [9].

### B. Twelve Topologies

Iron and non-magnetic cores can both be used in an SCSG. Using iron cores is more conventional and can reduce the magnetic reluctance of a machine and the amount of used superconductors. The downsides are large weights and extra losses. Using non-magnetic core can be applied to SC machines because the magnetic field excited by SC field windings can be very high. Usually non-magnetic cores are lightweight and loss free, but the magnetic reluctance of a machine would be so large that more superconductors have to be used to excite a sufficiently high magnetic field.

Combining iron and non-magnetic cores in the rotor back core, rotor pole core, stator tooth and stator yoke results in twelve applicable topologies (T1-T12) in total as given in Fig. 1. In this list, nine topologies T1-T3, T5-T7, and T9-T11 have a large effective air gap length due to space allocated to the cryostat wall and thermal insulation. The other three topologies T4, T8 and T12 with salient iron poles have a significantly reduced effective air gap length. Because in these three topologies, the cryostat is made modular in the shape of racetrack and the iron pole can go as close to the stator as possible [10]-[12], [13]. T4, T8 and T12 can be regarded as the extensions of T3, T7 and T11, respectively, from the topology point of view.

### C. Operation of Wind Turbine and Generator

The wind speed condition follows a Weibull distribution (shape factor  $k = 2$ , scaling factor  $A = 10.39$ ). The wind turbine operates following the rotational speed and power as a function of wind speed as shown in Fig. 2. The generator is operated under the phasor diagram given in Fig. 3, which is fully controlled by the power electronic converter. The phasor

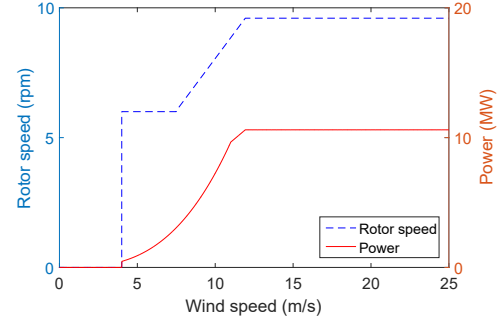


Fig. 2. Rotor speed and aerodynamic power of the reference wind turbine.

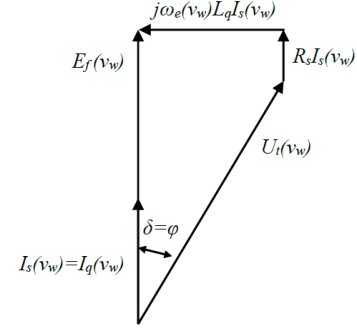


Fig. 3. Phasor diagram of the generator operating point, where  $v_w$  is wind speed. Voltages and currents are functions of wind speed.

diagram is applied with the zero d-axis control with which the d-axis current of the generator remains zero and the torque is proportional to the q-axis current. The major advantage of this control strategy is relatively low copper losses in the armature winding. This phasor diagram of generator operation is a starting point and other operations can be applied in future studies.

The superconducting field winding of an SCSG is prone to AC losses when the field current is regulated in the way a conventional electrically excited synchronous generator is regulated. Thus, the field current must be changed sufficiently slowly and is changed only for regulations in hours or days. In this paper, we assume a constant field current of rated value throughout the full range of wind speed to neglect the field current regulation process at partial load.

## III. CALCULATION OF CAPITAL COST OF ENERGY

In this paper, the capital CoE is defined by

$$CoE = \frac{C_{act} + C_{other}}{a \cdot AEP} \quad (1)$$

where  $C_{act}$  is the active material cost of the SCSG,  $AEP$  is the annual energy production, and  $a = 14.1$  is the annuity factor for a design life time of 25 years (assuming a 5% interest).

### A. Costs

Choice of topologies changes  $C_{act}$ . The other costs of the wind turbine  $C_{other}$  is assumed to be constant since  $C_{other}$  can hardly be changed by topology choice.

TABLE I  
ESTIMATION OF THE OTHER COSTS OF THE WIND TURBINE

Parameter	Cost	Reference
Wind turbine (excl. gen. system)	7,500 k€	Cost model in [1]
Balance of plant	17,000 k€	Cost model in [1]
Power electronics $C_{PE}$	800 k€	Cost model in [1]
Cryogenic system $C_{cryo}$	600 k€	LTS SCSG in [14]
Generator supporting structures $C_{str}$	880 k€	LTS SCSG in [14]
Total $C_{other}$	26,780 k€	-

1) *Active material cost*: the active materials under consideration and their unit costs are

- $MgB_2$  wires for the field winding (1 or 4 €/m, depending on the used scenario),
- copper conductors for the armature winding (15 €/kg),
- ferromagnetic core material (3 €/kg), and
- non-magnetic core material (i.e. glass fiber G10) (15 €/kg).

2) *Other costs*: The cost of each component of the wind turbine considered in  $C_{other}$  is given in Table I. The cryogenic system cost depends on a particular cryogenic design and can hardly be estimated by electromagnetic analyses, and the cost estimation for supporting structures needs detailed mechanical analyses. Here these two costs are estimated based on a 13.2 MW LTS SCSG in [14].

The cost model from the INNWIND.EU project defines a reference 10-MW wind turbine and estimates the cost of each wind turbine component [1]. The total cost excluding  $C_{act}$  is roughly 27,000 k€ which is given to (1) as  $C_{other}$ .

### B. Power Losses

For calculating the AEP, all power losses and then the output power from the generator system should be calculated. The input power to the generator system  $P_{in}$  is the shaft power from the hub of a wind turbine. Assuming that mechanical losses, e.g. bearing and windage losses, are neglected, the input power is determined by the aerodynamic power from wind:

$$P_{in} = 0.5\rho_{air}C_p\pi r_{tr}^2 v_w^3 \quad (2)$$

where  $\rho_{air}$  is the mass density of air,  $C_p$  is the power coefficient of a wind turbine,  $r_{tr}$  is the turbine rotor radius, and  $v_w$  is the wind speed.

The total loss of the generator system  $P_{Loss}$  is calculated by

$$P_{Loss} = P_{Cu,joul} + P_{Cu,eddy} + P_{Fe,s} + P_{cryo} + P_{conv} \quad (3)$$

where  $P_{Cu,joul}$  is the copper joule loss in the armature winding,  $P_{Cu,eddy}$  is the copper eddy current loss in the armature winding which is modeled in [15], and  $P_{Fe,s}$  is the iron loss in the armature iron core which is modeled in [16]. We assume that no losses exist in the field winding iron cores. The loss of the power electronic converter  $P_{conv}$  is modeled based on the current flowing in the power electronic switches and given in [16].

The losses, both DC and AC losses, in the superconducting winding are negligibly small, according to the study in [12].

Thus, these losses are not considered. The refrigeration for cooling the cryogenic environment for superconducting wires demands a power at an ambient temperature, which can also be considered as a power loss  $P_{cryo}$ . The cryogenic cooling power is estimated as 0.5% of the rated power of the superconducting generator. This estimation is based on the technical report by GE for an LTS SCSG design [17], which calculated the cryogenic cooling power at different wind speeds. This report shows that the cryogenic cooling power is constant with wind speed and its value is 22.5 kW. Here we assume a constant cryogenic cooling power of 50 kW at all wind speeds. This power value is more than doubled 22.5 kW to consider tolerances.

### IV. OPTIMIZATION

The optimization objective function is the capital CoE given in (1). Only the capital costs are considered. For dynamic stability of a 10-MW wind turbine, a small tower head mass may not be desired due to natural frequency issues. The generator mass is thus not part of the optimization objective. The optimization program combines finite element (FE) and analytical models. The FE models calculate magnetic fields and torques. The analytical models calculate power losses.

The optimization applies a genetic algorithm NSGA-II, so all the optimization variables can be integer and their step sizes of evolution can be manipulated. The number of individuals per generation is set to 50. Each individual is a set of the optimization variables values. The optimization process will proceed until all the individuals converge to the same minimum objective. Different initial individuals are used to check if the optimum is global. The detailed optimization method can be found in [18].

### V. SCENARIO STUDY

Considering the fast development of superconductor technology, four scenarios are defined regarding the unit cost and the performance of  $MgB_2$  wires:

- Original: cost 4 €/m, current density capability  $J_c$ ,
- Scenario 1: cost 1 €/m, current density capability  $J_c$ ,
- Scenario 2: cost 4 €/m, current density capability  $4J_c$ ,
- Scenario 3: cost 1 €/m, current density capability  $4J_c$ .

The original one is based on currently available commercial  $MgB_2$  wires (supplied by Columbus Superconductors). Scenario 1 expects a lower unit cost (1/4) and Scenario 2 expects a higher current density capability (4 times). Scenario 1 is also expected by the  $MgB_2$  wire manufacturer for near future when mass production is realized. Scenario 3 is considered for long terms since it expects both. Such a scenario study applies to all the topologies and can show prospects of each topology in future. This scenario study covers short-term and long-term expectations on  $MgB_2$  wires and can increase the adaptability of this paper.

### VI. COMPARISON RESULTS

The key PI of capital CoE and the other important PIs are obtained from the twelve optimized topologies for the four

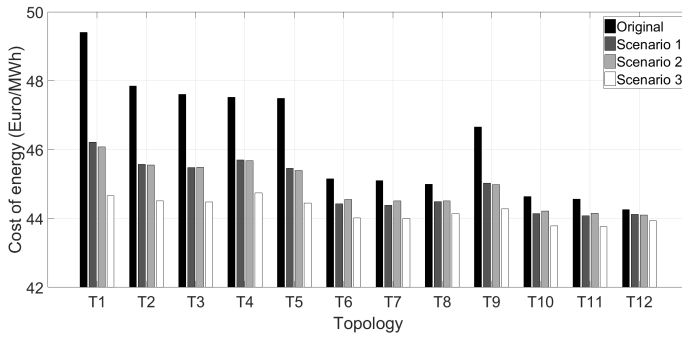


Fig. 4. Capital cost of energy.

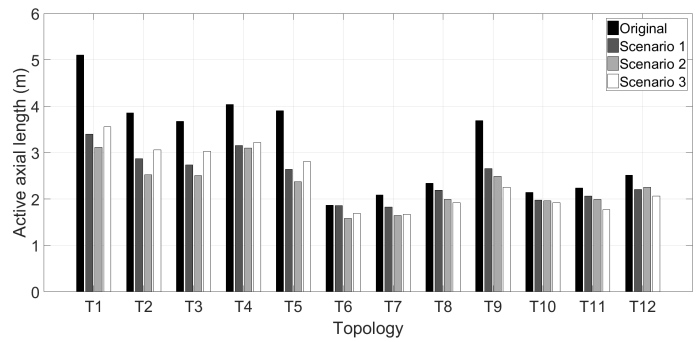


Fig. 7. Active generator length.

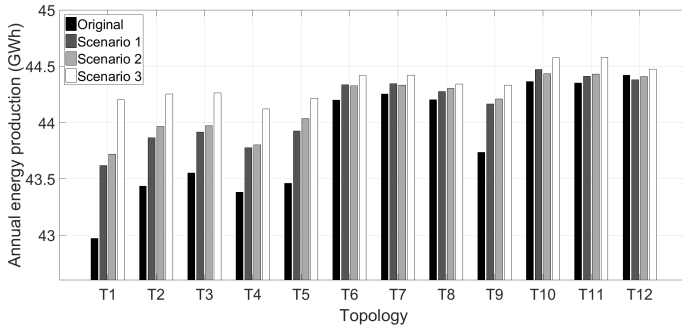


Fig. 5. Annual energy production.

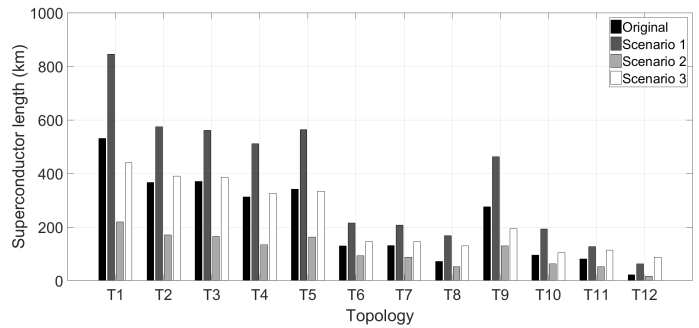


Fig. 8. Superconductor length.

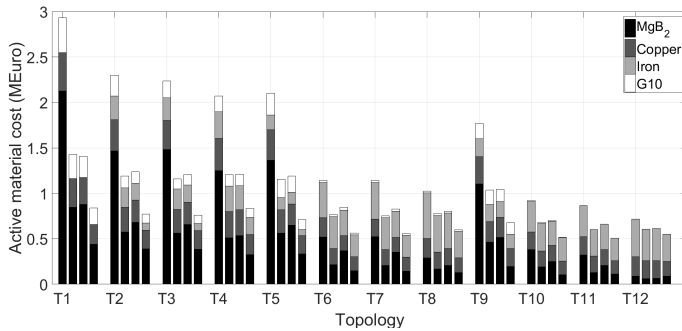


Fig. 6. Active material costs. Within a topology, the scenario changes from the left to the right.

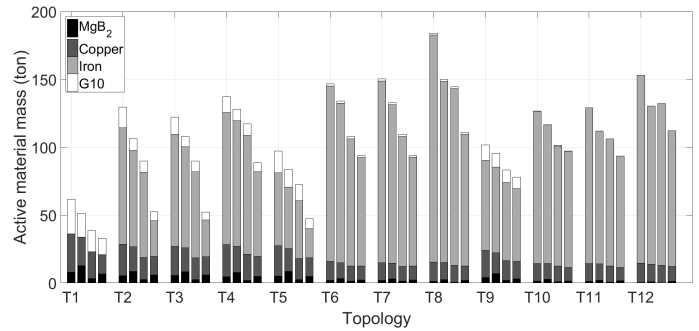


Fig. 9. Active material masses. Within a topology, the scenario changes from the left to the right.

scenarios. The optimum value of the design variables is given in Table II.

The capital CoE is compared in Fig. 4. T12 has the lowest capital CoE based on currently available  $MgB_2$  wires. Change of scenarios does not make significant differences for T12. T1-T5 and T9 are much more expensive than the other topologies in the original case. However, they will greatly benefit from the lower unit cost and the higher current density capabilities of  $MgB_2$  wires. Changing to Scenario 1-3 effectively reduce the distances of the capital CoE among the twelve topologies. Similar effects of changing scenarios can also be observed in the annual energy production as compared in Fig. 5 and in the active material cost as compared in Fig. 6. Scenario 3 results in the best performance regarding these three PIs. In summary, the topologies with more iron cores (T6-T8 and T10-T12) show advantages in the original cases while the topologies with more non-magnetic cores (T1-T5 and

T9) become competitive when the unit cost of  $MgB_2$  wires is reduced or the current density capability is enhanced. In addition, these three comparison results show that Scenarios 1 and 2 have similar PIs. In other words, either reducing the unit cost or increasing the capability of the  $MgB_2$  wires can reach the similar effects on the capital CoE, AEP and total active material cost.

The active generator length is compared in Fig. 7. T6 gives the shortest generator but change of scenarios does not make much difference. The topologies with more non-magnetic cores (T1-T5 and T9) also benefit from using Scenario 1-3. However, Scenario 3 is not the best anymore in T1-T6.

The superconductor length is compared in Fig. 8. T12 shows great advantages of reducing the used superconductor length in all the scenarios, which can facilitate manufacturing of the superconducting wire. As expected, cheaper  $MgB_2$  wires results in more use thereof. In general, more iron cores can

TABLE II  
OPTIMUM VALUE OF DESIGN VARIABLES.

	T1				T2				T3				T4			
	OR	S1	S2	S3												
$p$	12	12	12	12	12	12	14	12	14	12	14	12	12	12	12	12
$\alpha$ (°)	24	24	24	24	24	24	28	24	28	28	30	24	38	40	40	26
$\beta$ (°)	90	90	90	90	90	90	90	90	90	90	90	90	80	80	80	80
$h_f$ (mm)	16	36	10	18	14	28	10	18	16	30	10	18	18	38	10	18
$h_s$ (mm)	60	60	60	40	74	58	64	42	68	58	64	42	60	58	58	44
$h_{sy}$ (mm)	60	60	60	40	74	58	64	42	68	58	64	42	62	58	58	44
$h_{ry}$ (mm)	60	60	60	40	162	182	182	62	158	190	180	58	142	174	174	122
$b_t/\tau_s$	0.31	0.31	0.31	0.31	0.44	0.31	0.36	0.31	0.39	0.31	0.36	0.31	0.31	0.31	0.31	0.31
	T5				T6				T7				T8			
	OR	S1	S2	S3												
$p$	14	14	14	14	12	14	16	14	14	14	16	14	12	14	14	14
$\alpha$ (°)	28	28	28	28	34	28	42	30	36	30	46	30	54	50	56	28
$\beta$ (°)	90	90	90	90	90	90	90	90	90	90	90	90	80	78	78	78
$h_f$ (mm)	14	32	10	18	10	16	10	12	10	16	10	12	10	24	10	12
$h_s$ (mm)	66	66	64	50	58	56	66	52	58	56	64	52	52	54	56	50
$h_{sy}$ (mm)	92	114	120	52	240	228	226	206	218	226	216	206	228	198	210	204
$h_{ry}$ (mm)	92	114	120	52	240	210	180	116	222	210	178	116	222	178	196	124
$b_t/\tau_s$	0.37	0.37	0.36	0.36	0.31	0.36	0.41	0.36	0.36	0.36	0.41	0.36	0.31	0.36	0.36	0.36
	T9				T10				T11				T12			
	OR	S1	S2	S3												
$p$	18	20	20	22	22	20	24	20	22	24	24	20	20	22	24	18
$\alpha$ (°)	36	40	40	44	48	40	58	40	56	48	64	42	66	64	66	46
$\beta$ (°)	90	90	90	90	90	90	88	90	90	90	88	90	74	72	70	74
$h_f$ (mm)	14	34	10	18	10	18	10	10	10	14	10	12	10	34	18	14
$h_s$ (mm)	78	100	94	100	130	82	108	72	118	108	108	74	118	108	116	64
$h_{sy}$ (mm)	84	100	102	100	134	156	124	172	130	122	122	174	122	128	126	158
$h_{ry}$ (mm)	84	100	102	100	134	156	118	92	136	128	124	94	118	106	106	110
$b_t/\tau_s$	0.47	0.59	0.56	0.59	0.68	0.53	0.62	0.53	0.65	0.62	0.62	0.53	0.65	0.62	0.65	0.47

$p$ - number of pole pairs,  $\alpha$ - start angle of field coil in electrical degree,  $\beta$ - end angle of field coil in electrical degree,  $h_f$ - height of field coil,  $h_s$ - height of armature slot,  $h_{sy}$ - height of armature yoke,  $h_{ry}$ - height of field back core,  $b_t/\tau_s$ - ratio of tooth width to slot pitch.

effectively reduce the use of superconducting wires.

The active material mass is compared in Fig. 9. T1 is the lightest since it fully uses lightweight non-magnetic cores. In general, the topologies with more iron cores are heavier. However, the heaviest one is not T12 but T8 since T8 uses much more iron in the back cores to reduce the capital CoE. Change from the original case to Scenarios 1-3 in the order effectively reduces the active material mass for all the topologies.

## VII. CONCLUSION

For 10-MW wind turbines using SCSGs, twelve topologies for designing SCSGs have been compared in four scenarios, regarding the key PI capital CoE. Some other important PIs resulting from the capital-CoE-based optimal designs are also shown. With the currently available commercial MgB<sub>2</sub> wires, the topologies with more iron cores perform better in the conducted comparisons. The fully iron-cored topology T12 with salient poles is most promising regarding the capital CoE, AEP, active material cost and superconductor length, although its active material mass and active generator length are moderate.

The scenario study shows that reduction of the unit cost or enhancement of the current density capability of MgB<sub>2</sub> wires will be beneficial for all topologies especially those

with more non-magnetic cores. Comparing Scenarios 1 and 2 shows that reducing the unit cost or increasing the capability of MgB<sub>2</sub> wires can reach similar effects on the capital CoE, AEP and total active material cost. The distances among the topologies become smaller from the original case to Scenarios 1-3. Especially, Scenario 3 makes the topologies with more non-magnetic cores much more competitive. However, to drive the unit cost down or increase the current density capability of MgB<sub>2</sub> wires takes time. At present, iron-based topologies is most promising. In future, non-magnetic-core-based topologies will become competitive as long as the superconductor becomes sufficiently cheaper and better.

## ACKNOWLEDGMENT

This work is part of the INNWIND.EU project supported by the FP7 framework of EU, under grant agreement No. 308974.

## REFERENCES

- [1] (2016, September) INNWIND.EU official website. [Online] Available: <http://www.innwind.eu/>
- [2] A. B. Abrahamsen, N. Mijatovic, E. Seiler, T. Zirngibl, C. Træholt, P. B. Nørgård, N. F. Pedersen, N. H. Andersen and J. Østergård, "Superconducting wind turbine generators," *Supercond. Sci. and Technol.*, vol. 23, pp. 034019, 2010.
- [3] B. B. Jensen, N. Mijatovic, and A. B. Abrahamsen, "Development of superconducting wind turbine generators," *Journal of Renewable and Sustainable Energy*, vol. 5, pp. 023137, 2013.

- [4] H. Polinder, J. A. Ferreira, B. B. Jensen, A. B. Abrahamsen, K. Atallah, and R. a. McMahon, "Trends in wind turbine generator systems," *IEEE J. Emerg. Sel. Top. Power Electron.*, vol. 1, pp. 174185, 2013.
- [5] Ronghai Qu, Yingzhen Liu and Jin Wang, "Review of superconducting generator topologies for direct-drive wind turbines," *IEEE Trans. on Appl. Supercond.*, vol. 23, pp. 5201108, June 2013.
- [6] C. Lewis, and J. Muller, "A direct drive wind turbine HTS generator," *IEEE Power Engineering Society General Meeting*, pp. 1-8, 24-28 June 2007.
- [7] G. Snitchler, B. Gamble, C. King, and P. Winn, "10 MW class superconductor wind turbine generators", *IEEE Trans. on Appl. Supercond.*, vol. 21, pp. 10891092, 2011.
- [8] B. Maples, M. M. Hand, and W. D. Musial, "Comparative assessment of direct drive high temperature superconducting generators in multi-megawatt class wind turbines," Golden, CO: National Renewable Energy Laboratory, 2010.
- [9] Juha Pyrhonen, Tapani Jokinen, and Valeria Hrabovcova, *Design of Rotating Electrical Machines*, New York: Wiley, 2009.
- [10] Y. Xu, N. Maki, L. Fellow, and M. Izumi, "Electrical design study of 10-MW salient-pole wind turbine HTS synchronous generators," *IEEE Trans. on Appl. Supercond.*, vol. 24, pp. 1-6, Dec. 2014.
- [11] I. Marino et al., "Lightweight MgB<sub>2</sub> superconducting 10 MW wind generator," *Supercond. Sci. Technol.*, vol. 29, pp. 024005, Feb. 2016.
- [12] Dong Liu, H. Polinder, N. Magnusson, J. Schellevis, and A. B. Abrahamsen, "Ripple field AC losses in 10 MW wind turbine generators with a MgB<sub>2</sub> superconducting field winding," *IEEE Trans. on Appl. Supercond.*, vol. 26, no. 3, pp. 1-5, April 2016.
- [13] H. Karmaker, M. Ho, D. Kulkarni, "Comparison between different design topologies for multi-megawatt direct drive wind generators using improved second generation high temperature superconductors," *IEEE Trans. on Appl. Supercond.*, vol. 25, pp. 1-5, June 2015.
- [14] Y. Liu, R. Qu, J. Wang, H. Fang, X. Zhang and H. Chen, "Influences of Generator Parameters on Fault Current and Torque in a Large-Scale Superconducting Wind Generator," in *IEEE Transactions on Applied Superconductivity*, vol. 25, no. 6, pp. 1-9, Dec. 2015.
- [15] A. A. Arkadan, R. Vyas, J. G. Vaidya and M. J. Shah, "Effect of toothless stator design and core and stator conductors eddy current losses in permanent magnet generators," *IEEE Trans. on Energy Conversion*, vol. 7, pp. 231-237, March 1992.
- [16] H. Polinder, F. F. Van Der Pijl, G. J. De Vilder, and P. J. Tavner, "Comparison of direct-drive and geared generator concepts for wind turbines," *IEEE Trans. Energy Convers.*, vol. 21, no. 3, pp. 725733, 2006.
- [17] Fair, R. Superconductivity for Large Scale Wind Turbines, DOE report DE-EE0005143, 2012.
- [18] Dong Liu, H. Polinder, A. B. Abrahamsen and J. A. Ferreira, "Comparison of 10 MW superconducting generator topologies for direct-drive wind turbines," *IEEE International Electric Machines & Drives Conference*, Coeur D'Alene, USA, pp. 174-180, May 2015.